

Microwave study of quantum n -disk scattering

Wentao Lu, Lorenza Viola, Kristi Pance, Michael Rose, and S. Sridhar

Department of Physics

Northeastern University, Boston, Massachusetts 02115

(November 8, 2017)

We describe a wave-mechanical implementation of classically chaotic n -disk scattering based on thin 2-D microwave cavities. Two, three, and four-disk scattering are investigated in detail. The experiments, which are able to probe the stationary Green's function of the system, yield both frequencies and widths of the low-lying quantum resonances. The observed spectra are found to be in good agreement with calculations based on semiclassical periodic orbit theory. Wave-vector autocorrelation functions are analyzed for various scattering geometries, the small wave-vector behavior allowing one to extract the escape rate from the quantum repeller. Quantitative agreement is found with the value predicted from classical scattering theory. For intermediate energies, non-universal oscillations are detected in the autocorrelation function, reflecting the presence of periodic orbits.

I. INTRODUCTION

The system of n -disks on a plane is perhaps the simplest and paradigmatic example of a chaotic scattering system [1–5]. The classical differential cross-section of the system with $n > 2$ disks on a plane is singular, with singular points forming a Cantor set [1,3]. Thus, the investigation of chaotic scattering geometries naturally brings in the capability to access the intrinsic *fractal* nature of the underlying classical repeller.

From the perspective of quantum-classical correspondence, the wave-mechanical counterpart of this “fractal pinball game” is even more intriguing. Semiclassical attempts to treat this problem led to important theoretical advances and to the development of sophisticated semiclassical tools, notably cycle expansion, that represents one of the more productive applications of periodic orbit theory [5].

From a broader perspective, the n -disk scattering can be regarded as the prototype of an *open quantum chaos system*. For closed quantum chaotic systems (billiards in particular), theoretical and experimental results are available on spectral eigenvalues (which are purely real), and a good understanding of both universal and non-universal features has been reached [6]. Open chaotic systems are a special class of open quantum systems, whereby bound states of a closed geometry are converted to long-lived metastable states due to coupling to continua. Accordingly, eigenvalues are intrinsically complex and their universal behavior is currently a subject of considerable interest [7].

Investigation of n -disk scattering was originally stimulated by the attempt of modelling unimolecular reactions [3]. However, the system turns out to be a good exemplification for a variety of physical situations, ranging from crossroad geometries for semiconductor devices, to electromagnetic and acoustic scattering, and heavy-ion

nuclear reactions [8].

In spite of extensive theoretical analysis, there have been few direct experimental implementations of such chaotic model geometries so far. In this paper we present the results of a systematic experimental study of the quantum resonances and decay characteristic of 2-D scattering repellers. The experiments utilize thin microwave geometries where, under appropriate conditions, the underlying Helmholtz equation maps exactly into the time-independent Schrödinger equation in two dimensions. Experiments were carried out for $n = 1, 2, 3, 4$, as well as for large $n = 20$, the latter corresponding to the so-called random Lorentz scatterer. A concise account of the main results has been presented in [9].

The experiments, which are able to access the stationary Green's function of the system, yield the frequencies and the widths of the low-lying quantum resonances. We carried out semiclassical calculations of such resonances, which are found to reproduce the measured spectra reasonably well. Our experiments enable us to explore the role of symmetry in a unique way by probing different irreducible representations of the symmetry group of the scatterer. The experimental data are used to identify both universal and non-universal signatures of the classical chaos in the transmission spectra, through measures such as the spectral (wave-vector) autocorrelation function.

Correlation functions are a valuable tool to extract key information on the spectral properties of the system. In mesoscopic conductors, measurements of the magnetic field correlation of the conductivity have provided unique insight into the manifestations of the chaotic classical dynamics at the quantum level [10]. Correlations of wave functions in chaotic systems have been considered recently as a probe for classical ergodicity predictions [11]. In the present experiments, we take advantage of our ability to vary the wave-vector of the system to directly

access energy correlations, that are difficult to extract in semiconductor microstructures. The small k (long time) behavior of the resulting autocorrelation provides a measure of the *quantum escape rate*, which is shown to be in good agreement with the corresponding classical value. For large k (short time), the contribution of periodic orbits is evidenced through non-universal oscillations of the autocorrelation function.

The content of the paper is organized as follows. After describing the experimental realization in Sec. II, the connections between electromagnetic and quantum mechanical scattering, and between the observed transmission amplitude and the stationary Green's function are elucidated in Sec. III. In Sec. IV, the essential background on semiclassical theory is recalled, with emphasis on the role played by symmetry properties. The remaining sections are devoted to the presentation and the interpretation of the experimental results: in Sec. V, we present a comparison between the measured traces and the semiclassical predictions for various scattering geometries probed in the experiment, while in Sec. VI we focus on the analysis of spectral autocorrelations, from which the wave-mechanical escape rate can be extracted. An overall discussion of the results and their implications, together with an outlook on open issues and future work are presented in the conclusive section.

II. EXPERIMENTAL REALIZATION

The experiments were carried out in thin microwave structures consisting of two highly conducting Cu plates spaced $d \simeq 6$ mm and about 55×55 cm² in area. A picture of a typical experimental setup is displayed in Fig. 1. Similar experiments in *closed* geometries have provided direct observation of scars [12], enabled precise tests of eigenvalue statistics [13], and allowed experimental studies of localization effects [14]. Disks and bars also made of Cu and of thickness d were placed between the plates and in contact with them. Disks of radius $a = 2$ and $a = 5$ cm were used in the experiments. In order to simulate an infinite system, microwave absorber material was sandwiched between the plates at the edges. Microwaves were fed into the system by inserting a loop-terminating coaxial line in the vicinity of the scatterers. Since we ensure that the relation $f < f_c = c/2d = 25$ GHz is valid for all operating frequencies (here $k = 2\pi f/c$, c being the speed of light), the only allowed electromagnetic modes are a class of TM (Transverse Magnetic) modes with no variation along the direction z orthogonal to the plates. The nonvanishing field components for these states are the axial component of the electric field E_z , and transverse components of the magnetic field H_x, H_y , or $\mathbf{H} = (1/ik)\hat{z} \times \nabla E_z$. Thus, essentially, the geometry of the experiment can be regarded as 2-dimensional, the whole field configuration being accessible from knowl-

edge of E_z alone. The output signal can be picked up by both directly coupling to the axial electric field E_z (*electric coupling*) or by measuring the associated transverse magnetic field \mathbf{H} (*magnetic coupling*). In the first configuration, a microwave pin is inserted through appropriate holes drilled on the top plate of the cavity, while magnetic coupling is established by suitably positioning a second loop perpendicular to the plates. Note that, for a sufficiently small loop area, the measured signal is simply proportional to the electric field value at the pick-up probe location in both cases. Data from both electric and magnetic coupling configurations are used in the subsequent analysis.

The resonances were probed in the transmission mode by sweeping the frequency in the range between 0 and 20 GHz. All the measurements are carried out using an HP8510B vector network analyzer measuring the complex transmission coefficient $S_{21}(f) \equiv (X + iY)(f)$ of the coax plus scatterer system. It is crucial to ensure that there is no spurious background scattering due to the finite size of the system. This was verified carefully as well as that the effects of the coupling probes were minimal and did not affect the results. Also, we stress that dissipation effects due to finite conductivity of the walls are entirely negligible in the present experiments.

III. GREEN'S FUNCTION AND EXPERIMENTAL S -PARAMETERS

A. Electromagnetic vs. quantum mechanical scattering

According to Maxwell equations, the problem of stationary scattering of electromagnetic waves from perfect metallic conductors in a 2-D plane is defined mathematically by the Helmholtz equation for the field component

$$(\nabla^2 + k^2) E_z(\vec{r}) = 0, \quad (1)$$

for $\vec{r} = (x, y)$ outside the scattering region (*i.e.*, between the disks), supplemented by Dirichlet boundary conditions on the perimeter of any scatterer:

$$E_z(\vec{r}) = 0, \quad \vec{r} \in \text{perimeters}, \quad (2)$$

implying, for any geometry, a vanishing electric field inside the disks. The Helmholtz equation is formally identical to the time-independent Schrödinger equation with $\Psi = E_z$. Since, in addition, the same boundary conditions apply to both the axial electric field and the wavefunction, the problem is equivalent to quantum mechanical scattering from hard disks. This correspondence is exact in the whole range of frequencies below the cutoff frequency f_c that are considered in the experiment.

According to quantum scattering theory, the stationary properties of the scattering process are characterized

completely by the collection of S -matrix elements, expressing the transition amplitudes between asymptotic incoming and outgoing states [5,15]. The S -matrix exhibits poles as a function of the wave vector (or energy) of the incoming wave. These poles, corresponding to *scattering resonances*, occur in the complex k -plane, $k = k' + ik''$. The imaginary part is interpreted as a resonance width, implying that scattering resonances are associated with *metastable* states having a finite lifetime. Note that, in contrast to closed-cavity geometries where non-zero widths only arise due to the finite wall conductivity [16], widths have here a purely *geometric* origin, the openness of the system preventing a stable trapping of the states within the scattering geometry for arbitrarily long times. We shall use the convention $k = s - i\gamma$ for a given resonance, *i.e.*, $s = k'$ to denote the position of the resonance along the k -axis and $\gamma = -k''$, $k'' < 0$ to denote half-widths in the wave-vector domain. γ is related to the observed resonance width Δf in the frequency spectrum by $\Delta f = (c/2\pi) \Delta k = (c/2\pi) 2\gamma$.

The correspondence, pointed out above, between the equations of motion and the boundary conditions satisfied by electromagnetic (EM) and quantum-mechanical (QM) stationary scattering allows one to establish a direct mapping between the S -matrix spectral properties in the domain of *complex wave vectors*:

$$(k' + ik'')_{\text{EM}} = (k' + ik'')_{\text{QM}}. \quad (3)$$

This mapping enables us to study the quantum properties of the n -disk system. Note that quantum-mechanical (half) widths $\Gamma/2$ for unstable states are typically defined in the *energy* domain as $E = E' + iE'' = \varepsilon - i\Gamma/2$, $E'' < 0$, the relation between (complex) pseudo-energies and (complex) wave-vectors being $E = (\hbar k)^2/2m$ as in the real case [17], [18]. Thus, $E'' = (\hbar^2/m)k'k''$. However, due to the difference between the non-stationary propagators for EM and QM problems, care should be taken when introducing and comparing associated quantities like decay rates or lifetimes which are defined in the time domain. By exploiting the time-dependent Schrödinger equation, quantum decay rates for square amplitudes $|\Psi(t)|^2$ are found as inverse lifetimes $1/\tau = \Gamma/\hbar = |2E''|/\hbar$. One gets $\tau \cdot \Gamma/\hbar = 1$, expressing Heisenberg's uncertainty principle. From the full wave equation for a monochromatic field, the decay rate of the field amplitude $|E_z(t)|^2$ is given by $1/\tau = 2\gamma c = c|2k''|$. Accordingly, $\tau \cdot 2\gamma c = 1$. In spite of such a difference, the wave mechanical spectrum will allow us to extract a quantity (the classical escape rate) which is related to the average trapping time of the underlying classical trajectories inside the scattering region.

B. Green's function

We turn now to outline the relationship between the measured response S_{21} and the two-point Green function of the chaotic billiard. The equation of motion satisfied by the relevant field component E_z in the presence of a monochromatic driving at frequency ω is

$$\left(\nabla^2 - \frac{1}{c^2} \frac{\partial^2}{\partial t^2}\right) E_z(\vec{r}, t) = E_0(\vec{r}) e^{-i\omega t}, \quad (4)$$

\vec{r} denoting 2-D coordinates in the plane and $E_0(\vec{r})$ being the associated amplitude for waves fed into the cavity with wave vector $k = \omega/c$. For a stationary field configuration, the above equation reads

$$(\nabla^2 + k^2) E_z(\vec{r}) = E_0(\vec{r}). \quad (5)$$

By definition, the so-called Green's function (or propagator) associated with the wave equation differential operator satisfies the equation

$$\left(\nabla^2 - \frac{1}{c^2} \frac{\partial^2}{\partial t^2}\right) G(\vec{r}, \vec{r}_0; t, t_0) = \delta(\vec{r} - \vec{r}_0) \delta(t - t_0), \quad (6)$$

for fixed \vec{r}_0 and t_0 . The Green's function $G(\vec{r}, \vec{r}_0; t, t_0)$ is identical to the wavefunction generated by the system at point \vec{r} and time t in response to a delta-like excitation applied at point \vec{r}_0 and time t_0 . For a time-homogeneous system, $G(\vec{r}, \vec{r}_0; t, t_0) = G(\vec{r}, \vec{r}_0; t - t_0)$, and Fourier transformation of Eq. (6) gives

$$(\nabla^2 + k^2) G(\vec{r}, \vec{r}_0; k) = \delta(\vec{r} - \vec{r}_0), \quad (7)$$

where the stationary Green's function has been introduced:

$$G(\vec{r}, \vec{r}_0; t - t_0) = \frac{1}{2\pi} \int G(\vec{r}, \vec{r}_0; k) e^{ick(t-t_0)} dk. \quad (8)$$

Knowledge of the Green's function allows one to calculate the response of the system to a generic excitation $E_0(\vec{r})$ as a convolution integral $E_z(\vec{r}_2) = \int_V G(\vec{r}_2, \vec{r}; k) E_0(\vec{r}) d\vec{r}$. In particular, if a point-like probe is placed at \vec{r}_1 to excite the system, $E_0(\vec{r}) = E_0(\vec{r}_1) \delta(\vec{r} - \vec{r}_1)$, we simply get $E_z(\vec{r}_2) = G(\vec{r}_2, \vec{r}_1; k) E_0(\vec{r}_1)$.

The connection with the observable quantity of our experiments is established by recalling that the transmission coefficient $S_{21} = V_{out}/V_{in}$, where V_{in} and V_{out} are linear responses to the electric field at the probe locations \vec{r}_1 (input) and \vec{r}_2 (output) respectively. Note that S_{21} can be related to the S -matrix element describing transmission between waves entering through antenna 1 and going out through antenna 2 [19]. We have $V_{out} = \alpha E_z(\vec{r}_2)$, $V_{in} = \beta E_0(\vec{r}_1)$, α and β denoting impedance factors that are characteristic of the coax lines and the analyzer, and are generally slowly-varying functions of frequency. Thus we get $S_{21} = (\alpha/\beta) G(\vec{r}_2, \vec{r}_1; k)$, which we can write in the form

$$S_{21}(k) = A(k) G(\vec{r}_2, \vec{r}_1; k). \quad (9)$$

In a formal analogy with the closed-system case, the Green's function can be expressed in terms of a generalized eigenfunction expansion [17],

$$G(\vec{r}_2, \vec{r}_1; k) = \sum_n \frac{\Psi_n(\vec{r}_2) \Phi_n^*(\vec{r}_1)}{k_n^2 - k^2}, \quad (10)$$

$\Psi_n(\vec{r})$ denoting the n -th eigenfunction of an effective open-system Hamiltonian, with corresponding adjoint eigenstate $\Phi_n(\vec{r})$ and associated (complex) wave vector k_n . It is worth stressing that the measured Green's function is identical with the actual Green's function of the open system provided the perturbation introduced by the probes is negligible. If this is not the case, a modified Green's function is generally obtained, with *shifted* complex poles in the expansion (10) (*i.e.*, resonances are shifted and broadened due to the presence of the probes). In the experiment, we ensured that the antennas were only *weakly* coupled to the system, with associated perturbation effects less than $\approx 10^{-3}$ of the observed frequencies and widths. Under these conditions, the relation established above between S_{21} and the Green's function generalizes the derivation for closed microwave billiards presented in [19].

C. Comparison with mesoscopic conductivity measurements

The connection between so-called transmission function, S -matrix, and Green's function is well known in the field of mesoscopic transport [17]. In particular, we recall that the *transmission function* of a coherent conductor between two leads 1, 2 is defined as [20]

$$T = \sum_{m \in 1, n \in 2} |t_{mn}|^2, \quad (11)$$

where the transmission coefficient t_{mn} , which characterizes the transmission amplitude between mode m in lead 1 and mode n in lead 2, is given by

$$t_{mn} = -i\hbar\sqrt{v_m v_n} \int dy' dy \phi_m^*(y') \phi_n(y) G(y', x_2, y, x_1; k). \quad (12)$$

Here, v_m (v_n) and ϕ_m (ϕ_n) are the longitudinal velocity and the transverse wave function for the mode m in lead 1 (n in lead 2) respectively, while $x_{1(2)}$ denote the longitudinal coordinate of antennas 1, 2. The transmission coefficients, which are clearly energy (frequency) dependent, are directly related to the correspondent elements of the S -matrix. In fact, the above expression for t_{mn} is a two-probe version of the general connection known as the Fisher-Lee relation between the S -matrix and the Green's

function [21]. The transmission T is related directly to the *conductance* σ of the conductor by the Landauer formula, $\sigma = (e^2/h) T$, e denoting the electron charge [17].

In the case of a point-like excitation and a point-like probing of the system, the input/output leads act as zero-dimensional tunneling point contacts. Thus, the transverse dimension of the leads can be neglected and the wave functions $\phi_m(y)$ in Eq. (12) are proportional to δ -functions, $\phi_m(y') = \delta(y' - y_2)$, $\phi_n(y) = \delta(y - y_1)$. By combining the two expressions above, and putting $\vec{r}_1 = (x_1, y_1)$, $\vec{r}_2 = (x_2, y_2)$, we get $T(k) \propto |G(\vec{r}_2, \vec{r}_1, k)|^2$. Since the Green's function is directly related, as shown in the previous section, to the experimental trace, one can interpret

$$T(k) \propto |S_{21}(k)|^2 \quad (13)$$

as a measurement of the two-point conductance. As a consequence, direct comparison is possible with theories originally developed for electronic micro-structures [10,20,22,23]. Note that in the language of mesoscopic conductors, the weak-coupling assumption between the system and the point-like leads implies the possibility of neglecting, as noticed above, any perturbation effect associated with the so-called lead self-energy [17]. From a general point of view, microwave-based implementations offer, compared to their solid-state counterparts, the advantage of a simple and practically unlimited manipulation of geometrical properties, along with the possibility of changing the wave-vector (and thereby the energy) of the incoming waves at will. Lastly, since electromagnetic waves are intrinsically non-interacting, a direct analogy with the ideal limit of a non-interacting electron gas applies and microwave experiments automatically probe quantum transport in the ballistic regime.

IV. SEMICLASSICAL THEORY

The starting point for the semiclassical derivation is the concept of generalized density of states $D(E)$ which, according to Balian and Bloch [24], is defined as a suitable difference between the density of states of the free and of the scattering system. The relative density of states is related to the S -matrix in the following way:

$$D(E) = \frac{1}{2\pi i} \text{tr} \left[S^\dagger \frac{dS(E)}{dE} \right]. \quad (14)$$

Therefore, the density $D(E)$ and the S -matrix share the same complex poles. $D(E)$ itself is written as

$$D(E) = -\frac{1}{\pi} \text{Im} g(E), \quad (15)$$

where the function $g(E)$, which is related to the so-called quantum Selberg zeta function, is the trace of the difference between the Green's function in the presence and in the absence of the disks respectively.

In the semiclassical limit, $g(E)$ is expressed as a sum over periodic orbits *i.e.*, by Gutzwiller's trace formula [25]. The trace function can then be written in terms of the Ruelle ζ -function as [3],

$$g(E) = g_0 - \sum_{j=0}^{\infty} \frac{\partial}{\partial E} \ln \zeta_{(1/2)+j}(-ik), \quad (16)$$

where g_0 , which is independent on the energy E , is given by the difference between the so-called Thomas-Fermi state densities with and without the disks, *e.g.*, $g_0 = -4a^2m/(2\hbar^2)$ in the 4-disk configuration. In Eq. (16), the Ruelle ζ -function with j running from 0 to ∞ is given explicitly as

$$\zeta_{(1/2)+j}(-ik) = \prod_p \left[1 - (-1)^{L_p} e^{ikl_p} / \Lambda_p^{(1/2)+j} \right]^{-1}, \quad (17)$$

where k is the wave vector, l_p is the length of the periodic orbit p , L_p the number of collisions of the periodic orbit with the disks, and Λ_p the eigenvalue of the so-called *stability* (or *monodromy matrix*). According to the above expressions, the task of finding the scattering resonances of the system is reduced to the problem of identifying the complex poles of the Ruelle ζ -function. Since the Ruelle ζ -function with $j = 0$ provides the leading contributions to the resonances with longer lifetimes (sharper resonances), we will only restrict ourselves to this case in our subsequent discussion.

The Ruelle ζ -function can be conveniently expressed in terms of a so-called *Euler product representation*,

$$\zeta^{-1} = \prod_p (1 - t_p), \quad (18)$$

t_p denoting the semiclassical weight for cycle p [26]. In practice, the periodic orbit formula for the Ruelle function is evaluated by performing a *cycle expansion* and investigating the zeros and radii of convergence as functions of truncations to cycles of a given maximum topological length. In the n -disk problem, if the disks are positioned sufficiently far from each other along a ring, it is possible to travel between any three successive of them and the trapped trajectories can be put in one-to-one correspondence with the bi-infinite sequence of symbols ω_k taken in the alphabet $\{1, 2, 3, \dots, n\}$ with $\omega_{k+1} \neq \omega_k$. The latter constraint implies that the topological entropy per bounce is equal to $\ln(n-1)$. Thus, the system symbolic dynamics has a finite grammar and the Euler product (18) can be rewritten by separating out a dominant fundamental contribution and the remaining corrective terms:

$$\prod_p (1 - t_p) = 1 - \sum_f t_f - \sum_r c_r. \quad (19)$$

Here, the number of fundamental terms t_f is equal to the number of symbols in the unconstrained symbolic

dynamics, while the so-called *curvature corrections* c_r represent contributions due to the nonuniformity of the system [26].

In our experiments, n identical disks are placed on a ring with equal space between the nearest neighbors. Accordingly, the system is characterized by symmetry point group $G = C_{2v}, C_{3v}, C_{4v}, C_{5v}, C_{6v}, \dots$ for $n = 2, 3, 4$, *etc.*, and symmetry properties can be used to classify the corresponding scattering resonances. In practice, the presence of symmetries can also be exploited to simplify the cycle expansion and improve its convergence. The key concept is to remove symmetry-induced degeneracies between cycles by reducing the dynamics to the so-called *fundamental domain (FD)*. The latter is a region obtained by ideally replacing the symmetry axes with perfectly reflecting mirrors. Global periodic orbits of the full system can be described completely by folding irreducible segments into periodic orbits in the fundamental domain. Correspondingly, the Ruelle ζ -function can be factorized in the product over different irreducible representations (*irreps*) of the symmetry group [26]. By taking into account the degeneracies of the periodic orbits and working in the fundamental domain, the Euler product (18) takes the form

$$\prod_p (1 - t_p) = \prod_{\tilde{p}} (1 - t_{\tilde{p}}^{h_p})^{m_p}, \quad (20)$$

where a modified semiclassical weight has been introduced:

$$t_{\tilde{p}} = t_p^{1/h_p} = \frac{(-1)^{L_{\tilde{p}}}}{\sqrt{\Lambda_{\tilde{p}}}} \exp(ikl_{\tilde{p}}). \quad (21)$$

In Eqs. (20)-(21), $m_p = g/h_p$, g and h_p denoting respectively the order of the full symmetry group G and of the maximal subgroup leaving p invariant. \tilde{p} is the irreducible segment of the orbit p that corresponds to a fundamental domain orbit, $L_{\tilde{p}}$ is the number of collisions with the disk in the fundamental domain and $\Lambda_{\tilde{p}} = \Lambda_p^{1/h_p}$ the eigenvalue of the stability matrix in the fundamental domain. The calculation of $\Lambda_{\tilde{p}}$ can be easily performed by diagonalizing the stability matrix $J_{\tilde{p}}$ which, for hard-disk billiards, reads as [26,27]

$$J_{\tilde{p}} = (-1)^{n_{\tilde{p}}} \prod_{k=1}^{n_{\tilde{p}}} \begin{pmatrix} 1 & l_k \\ 0 & 1 \end{pmatrix} \begin{pmatrix} 1 & 0 \\ r_k & 1 \end{pmatrix}. \quad (22)$$

Here, for simplicity we rescaled the constant velocity to unit value. l_k denotes the length of the k -th free-flight segment of the cycle \tilde{p} , while $r_k = 2/a \cos \phi_k$ is the defocusing due to the k -th reflection, occurring at an incidence angle ϕ_k .

By construction, only one irreducible representation appears whenever the system is probed in the fundamental domain. Note that, in practice, one can easily

switch from one symmetry to another by varying the angle $\theta = \pi/n$. We recall now some relevant formulas for the symmetry configurations examined in the experiment.

A. C_2 factorization

The group $G = C_{2v}$ is the appropriate symmetry group for two-disk scattering which, without being chaotic, offers the most important example of a nontrivial *integrable* scattering problem. An exact analytical solution is available for the classical dynamics [28], while a full quantum mechanical calculation of the scattering resonances has been performed in [29,31]. From the standpoint of the semiclassical analysis, the symmetry group of the periodic orbits is $G = C_2$, characterizing the transformation properties of the orbits under the exchange of the two disks [29]. The fundamental domain is the half-space containing a single disk. There are just two group elements, $C_2 = \{e, P\}$, e being the identity and P the parity operation, and only one periodic orbit. Cycles classify according to the two irreducible representations A_1 (symmetric) and A_2 (antisymmetric). Let a and R denote the radius and the center-center disk separation respectively, with the ratio $\sigma \equiv R/a$. We have

$$\zeta_{A_1}^{-1} = 1 - t_0 \quad \zeta_{A_2}^{-1} = 1 + t_0, \quad (23)$$

with $t_0 = -\exp[ik(R-2a)]/\sqrt{\Lambda}$, and

$$\Lambda = (\sigma - 1) + \sqrt{\sigma(\sigma - 2)}, \quad (24)$$

denoting the eigenvalue of the monodromy matrix indicated above.

We thus get the semiclassical scattering resonances as

$$k_n = \frac{(2n - m)\pi - \frac{i}{2} \ln \Lambda}{R - 2a}, \quad n = 1, 2, \dots, \quad (25)$$

where $m = 1$ for the A_1 -irrep, $m = 0$ for the A_2 -irrep. In the fundamental domain, only the antisymmetric A_2 representation contributes.

B. C_{3v} factorization

The symmetric three-disk pinball is invariant under the transformations of the group C_{3v} . In addition to the identity transformation, they include two rotations through $2\pi/3$ and $4\pi/3$ about the main axis, and three mirror reflections around the symmetry axes. The fundamental domain is bounded by a disk and the two adjacent sections of the symmetry axes acting as mirrors (1/6th of the full space, see Fig. 3, inset). C_{3v} has two 1-D irreps A_1 and A_2 (symmetric and antisymmetric under reflections respectively), and one 2-D irrep of mixed symmetry

labelled E . The 3-disk dynamical zeta function factorizes into: $\zeta = \zeta_{A_1} \zeta_{A_2} \zeta_E^2$, the contributions of each given irreducible representation being given by the following curvature expansion [26]:

$$\zeta_{A_1}^{-1} = 1 - t_0 - t_1 - (t_{01} - t_0 t_1) - [(t_{001} - t_0 t_{01}) + (t_{011} - t_1 t_{01})] - \dots, \quad (26)$$

for the A_1 subspace,

$$\zeta_{A_2}^{-1} = 1 + t_0 - t_1 + (t_{01} - t_0 t_1) - [(t_{001} - t_0 t_{01}) - (t_{011} - t_1 t_{01})] - \dots, \quad (27)$$

for the antisymmetric A_2 subspace, and, for the mixed-symmetry subspace E ,

$$\zeta_E^{-1} = 1 + t_1 - (t_0^2 - t_1^2) + (t_{001} - t_1 t_0^2) + [t_{0011} + (t_{001} - t_1 t_0^2)t_1 - t_{01}^2] + \dots. \quad (28)$$

The representation in the fundamental domain is A_2 . A detailed comparison between the semiclassical predictions and the exact quantum resonances for the 3-disk scattering problem has been reported in [3,30]. Exact quantum calculation was also performed in [31].

C. C_{4v} factorization

The scattering problem of four equal disks placed on the vertices of a square is characterized by C_{4v} symmetry. This is a group consisting of the identity, two reflections across the coordinate axes, two diagonal reflections, and three rotations by angles $\pi/2, \pi$ and $3\pi/2$. The fundamental domain is a sector delimited by a disk, a portion of the corresponding diagonal axis and a portion of the concurrent coordinate axis (*i.e.*, 1/8th of the full space, see Fig. 4b, inset). C_{4v} has four 1-D irreps, either symmetric (A_1) or antisymmetric (A_2) under both types of reflections, or symmetric under one and antisymmetric under the other (B_1, B_2), and one 2-D representation E . The ζ -function is factorized as $\zeta = \zeta_{A_1} \zeta_{A_2} \zeta_{B_1} \zeta_{B_2} \zeta_E^2$, where the contributions for the various invariant subspaces have the following curvature expansion [26]:

$$\begin{aligned} \zeta_{A_1}^{-1} &= 1 - t_0 - t_1 - t_2 \\ &\quad - (t_{01} - t_0 t_1 + t_{02} - t_0 t_2 + t_{12} - t_1 t_2) \\ &\quad - (t_{001} - t_0 t_{01}) - (t_{002} - t_0 t_{02}) - (t_{011} - t_1 t_{01}) \\ &\quad - (t_{022} - t_2 t_{02}) - (t_{112} - t_1 t_{12}) - (t_{122} - t_2 t_{12}) \\ &\quad - (t_{012} + t_{021} + t_0 t_1 t_2 - t_0 t_{12} - t_1 t_{02} - t_2 t_{01}) \dots, \\ \zeta_{A_2}^{-1} &= 1 + t_0 - t_1 + (t_{01} - t_0 t_1) + t_{02} - t_{12} \\ &\quad - (t_{001} - t_0 t_{01}) - (t_{002} - t_0 t_{02}) + (t_{011} - t_1 t_{01}) \\ &\quad + t_{022} - t_{122} - (t_{112} - t_1 t_{12}) \\ &\quad + (t_{012} + t_{021} - t_0 t_{12} - t_1 t_{02}) \dots, \\ \zeta_{B_1}^{-1} &= 1 - t_0 + t_1 + (t_{01} - t_0 t_1) - t_{02} + t_{12} \end{aligned}$$

$$\begin{aligned}
&+(t_{001} - t_0 t_{01}) - (t_{002} - t_0 t_{02}) - (t_{011} - t_1 t_{01}) \\
&-t_{022} + t_{122} - (t_{112} - t_1 t_{12}) \quad (29) \\
&+(t_{012} + t_{021} - t_0 t_{12} - t_1 t_{02}) \dots,
\end{aligned}$$

$$\begin{aligned}
\zeta_{B_2}^{-1} &= 1 + t_0 + t_1 - t_2 \\
&- (t_{01} - t_0 t_1) + (t_{02} - t_0 t_2) + (t_{12} - t_1 t_2) \\
&+(t_{001} - t_0 t_{01}) - (t_{002} - t_0 t_{02}) + (t_{011} - t_1 t_{01}) \\
&+(t_{022} - t_2 t_{02}) - (t_{112} - t_1 t_{12}) + (t_{122} - t_2 t_{12}) \\
&- (t_{012} + t_{021} + t_0 t_1 t_2 - t_0 t_{12} - t_1 t_{02} - t_2 t_{01}) \dots, \\
\zeta_E^{-1} &= 1 + t_2 - (t_0^2 - t_1^2) + (2t_{002} - t_2 t_0^2 - 2t_{112} - t_2 t_1^2) \\
&+(2t_{0011} - 2t_{0022} + 2t_2 t_{002} - t_{01}^2 - t_{02}^2) \\
&+ 2t_{1122} - 2t_2 t_{112} + t_{12}^2 - t_0^2 t_1^2) \dots.
\end{aligned}$$

The representation in the fundamental domain is B_2 . A detailed comparison between the semiclassical predictions and the exact quantum resonances for the 4-disk scattering problem has been performed by [27].

V. COMPARISON WITH EXPERIMENTAL RESONANCES

The experimental transmission function $|S_{21}(k)|^2 = X^2(k) + Y^2(k)$ (Sec. II) can be expressed as a superposition of Lorentzian peaks,

$$|S_{21}(k)|^2 = \sum_i \frac{c_i \gamma_i}{(k - s_i)^2 + \gamma_i^2}, \quad (30)$$

where, as above, s_i , γ_i denote respectively the position and the half-width of the resonances in the k -domain. The parameters c_i are coupling coefficients that depend on the location of the two probes and reflect the coupling between the pick-up antenna with the E_z -pattern of a given resonant mode. Semiclassical calculations using the appropriate cycle expansion described in the previous section were performed for different geometries, leading to the real and imaginary part s_i and γ_i of the resonances. In comparing with the observed traces, the parameters c_i were set manually to fit the data. For a given scattering geometry, the trace S_{21} used is the average of several traces collected at different probe locations in order to avoid missing resonances due to the accidental coincidence of either probe with a node of the wavefunction. In general, good agreement is found for the resonant frequencies of relatively sharp resonances (with typical quality factors in the range $Q = f/\Delta f \lesssim 50$). Broader resonances with larger imaginary parts are instead not easy to distinguish, although all resonances are always contributing to the transmission function. We examine now specific configurations.

2-disk: For the two-disk scattering, preliminary measurements were reported in [32]. We carried out experiments in both the full and in the half-space geometry, with $a = 5$ cm and $R = 40$ cm. According to the discussion in Sec. IVa, the trace is expected to exhibit

resonance peaks at regularly spaced locations, $f_n = n$ GHz, $n = 1, 2, \dots$, with a constant width approximately equal to $\Delta f_n \simeq 0.29$ GHz (from Eq. (25)). A typical experimental trace is shown in Fig. 2, where we focussed on the A_2 -resonances between 0 and 20 GHz. The corresponding calculated trace is depicted as a dashed line. The agreement is found to be quite good for both the resonances and their width. The regularity of such a spectrum will manifest clearly in the corresponding autocorrelation function.

3-disk: For the 3-disk geometry, we recall that a first demonstration of classical chaotic scattering via scattering of laser light was presented in [33]. A typical microwave trace for a 3-disk scatterer with $\sigma = 4\sqrt{3}$ is presented in Fig. 3. Again, we focus on the fundamental domain representation of the scattering geometry, corresponding to resonances with A_2 -symmetry. The semiclassical calculations, which are shown as a dashed line, are carried out by using the cycle expansion (17) with 8 periodic orbits up to period 4. We verified that they accurately reproduce previous calculations on the same system [34,30]. For this scattering geometry, comparison with the exact quantum mechanical calculations is also available [31], implying a stringent test for the validity of the semiclassical method. According to Fig. 3, the overall agreement is qualitatively good, especially for the locations of the sharper resonances.

4-disk: The traces of a 4-disk scatterer with $\sigma = 4$ in the full space and the fundamental domain are shown in Fig. 4 top and bottom, respectively. Semiclassical calculations (dashed line) were performed by including a total of 14 periodic orbits up to period 3 along the same procedure adopted in [27]. Resonances belonging to different symmetry characters can be identified in the full-space configuration and compared with the semiclassical predictions [27]. A similar comparison can be performed in the fundamental domain, only based on resonances in the B_2 subspace. As for the 3-disk case, the semiclassical theory provides a qualitatively fair prediction of the resonance frequencies. We observe that, in general, the agreement for the lowest-energy widths is not as satisfactory, with discrepancies increasing with decreasing frequencies. This kind of discrepancy, which is also found in the 3-disk geometry discussed above, is intrinsic to the semiclassical calculation because of the large correction of the stationary phase approximation [29]. For the 3-disk [3,30,31] and 4-disk [27] systems, where exact quantum-mechanical calculations are available, the very low-lying resonance widths of semiclassical resonances appear to be systematically smaller (up to a factor 3) compared to the corresponding quantum ones.

A few general remarks are in order. Although the agreement between the experimental scattering resonances and the corresponding semiclassical predictions is generally within a few percents ($\approx 5\%$), some discrepancies are also evidenced from the data we analyzed.

Such discrepancies may manifest in the form of both frequency shifts or width modifications of the predicted resonances as well as in the presence of additional peaks in the experimental trace. Various mechanisms and experimental limitations are expected to contribute as possible sources of errors, including: symmetry-breaking perturbations introduced by non-perfect geometries, effects associated with spurious reflections, non-idealities in the operations of the microwave absorbers (*e.g.*, frequency-dependent response), or slight height variations over the cavity area. The combined action of such mechanisms makes open-geometry microwave experiments comparatively more demanding with respect to their closed-cavity counterpart, where some of the above error sources are practically irrelevant. While a deeper understanding of the unavoidable non-idealities faced by the experiments, along with the necessary technical improvements, are likely to be necessary for establishing a fully quantitative detailed comparison, the level of agreement reached in our present investigation can be considered a very satisfactory match with the opportunity of retaining a relatively simple experimental methodology.

VI. SPECTRAL AUTOCORRELATION

We now turn to analyze the data in terms of the so-called *spectral autocorrelation function*, which was calculated as

$$C(\kappa) = \langle |S_{21}(k - (\kappa/2))|^2 |S_{21}(k + (\kappa/2))|^2 \rangle_k. \quad (31)$$

Here, κ is the wave-vector difference and $\langle \rangle_k$ denotes an average over a band of wave-vectors centered at some value $k = k_0$ and of width Δk , the latter being large enough to include an appreciable number of resonances. The average (31) also includes a suitable window function which is chosen as [35]

$$f(x) = \begin{cases} 1 - |x|/\sqrt{6} & |x| < \sqrt{6} \\ 0 & |x| \geq \sqrt{6} \end{cases}, \quad x = \frac{k - k_0}{\Delta k}. \quad (32)$$

Besides its intrinsic interest, an additional motivation for investigating the properties of $C(\kappa)$ comes from the correspondence, pointed out in Sec. IIIc, with experiments performed on mesoscopic transport. For ballistic conductors, a formally similar magnetic-field correlation function received extensive theoretical and experimental attention as a potential probe for quantum chaos [10,35]. A similar autocorrelation measure was also considered recently in the context of molecular photodissociation spectra [36]. In our microwave experiments, the wave-vector plays the role of the magnetic field and since $|S_{21}(k)|^2 \propto T(k)$, the function $C(\kappa)$ can be regarded as a measure of the wave-vector correlations of the two-probe conductance. The dependence of the autocorrelation function on both the finite window Δk and the

center point k_0 has been checked in the calculations. We consider the average of autocorrelations with a different k_0 to compensate for slight dependences on the center point. Plots of typical experimental autocorrelations for 2-, 3-, and 4-disk systems are shown in Fig. 5, Fig. 6 and Fig. 7 respectively.

By inserting the explicit representation of $|S_{21}(k)|^2$ as a sum of Lorentzians, Eq. (30), the autocorrelation is found as

$$C(\kappa) = \pi \sum_{i,j} \frac{c_i c_j (\gamma_i + \gamma_j)}{(\kappa - (s_i - s_j))^2 + (\gamma_i + \gamma_j)^2}. \quad (33)$$

In a regime where there are no overlapping resonances, $|s_i - s_j| \gg (\gamma_i + \gamma_j)$, and the small- κ behavior of the autocorrelation can be simplified as [34]

$$C(\kappa) \approx \pi \sum_i \frac{2 c_i^2 \gamma_i}{\kappa^2 + 4\gamma_i^2}. \quad (34)$$

By exploiting a result from semiclassical Random Matrix Theory, the above sum can be replaced by a single Lorentzian [37,38]:

$$C(\kappa) = C(0) \frac{1}{1 + (\kappa/\gamma)^2}, \quad (35)$$

where the parameter $\gamma = \gamma_{cl}$ is identified with the *classical escape rate* from the chaotic scattering region, with the velocity scaled to 1. Accordingly, one can interpret the width of the autocorrelation function as an *average width* (and thereby lifetime) of the resonances [39,40].

A. Universal features: classical escape rate

According to the above predictions, a *universal* behavior of the the autocorrelation function is expected for sufficiently *small* correlation scales, regardless of the details of the geometry and the way the system is excited. Such universal behavior is captured by the single classical parameter γ . We recall its definition. Classically, if we shoot particles towards the scatterer, the number $N(t)$ of particles remaining in the scattering region after time t decays exponentially as

$$N(t) = N(0) \exp(-\tilde{\gamma}_{cl} t), \quad (36)$$

where $\tilde{\gamma}_{cl} = \lambda(1 - d)$ is the classical escape rate, λ is the Lyapunov exponent of the manifold of infinitely trapped orbits (strange repeller), and d is the information dimension of the unstable manifolds. The scaled escape rate, corresponding to unit velocity, is defined as $\gamma_{cl} = \tilde{\gamma}_{cl}/v$, v being the speed of the particles. The classical escape rate can be calculated through the *classical* Ruelle ζ -function [4,5],

$$\zeta_\beta(s) = \prod_p [1 - (-1)^{L_p} \exp(s l_p) / \Lambda_p^\beta]^{-1}, \quad (37)$$

which is analytical in the half-plane $\text{Res} < -P(\beta)$, and has poles in the other half-plane. In particular, $\zeta_\beta(s)$ has a simple pole at $s = P(\beta)$. Here, $P(\beta)$ is the so-called Ruelle topological pressure, from which all the characteristic quantities of classical dynamics can be derived in principle. The classical escape rate is $\gamma_{cl} = -P(1)$.

For the various scattering geometries investigated experimentally, we calculated the appropriate autocorrelation function from the observed trace and fitted the small- κ portion of the resulting curve with the Lorentzian behavior (35), thereby extracting an experimental escape rate γ_{qm} . In general, good agreement is observed with the classical prediction γ_{cl} , implying that in the regime of universality *the characteristic scale of wave-vector correlations in the measured two-point quantum conductance is well reproduced by knowledge of the chaotic classical scattering dynamics*, through the classical escape rate γ_{cl} .

2-disk: For the integrable two-disk system, the information dimension $d = 0$, thus $\tilde{\gamma}_{cl} = \lambda$. For unit velocity and $R > 2a$, we get [5]

$$\gamma_{cl} = \lambda = \frac{1}{R - 2a} \ln \Lambda, \quad (38)$$

$\Lambda \equiv \Lambda(\sigma)$ being the eigenvalue of the monodromy matrix introduced in Eq. (24). The autocorrelation for the experimental set up with $a = 5$ cm, $R = 40$ cm ($\sigma = 8$) is shown in Fig. 5. A value $\gamma_{qm} = 0.083$ cm⁻¹ is found, which is in excellent agreement with the classical result $\gamma_{cl} = 0.088$ cm⁻¹.

3-disk: For the three-disk scatterer, we have [5]

$$\gamma_{cl} \simeq \frac{1}{R} \ln(1.072 \sigma). \quad (39)$$

A representative wave-vector autocorrelation function for this system is displayed in Fig. 3, where the fundamental domain configuration has been investigated with $a = 5$ cm and $R = 20\sqrt{3}$ cm. From equation (39), $\gamma_{cl} \simeq 0.058$ cm⁻¹, to be compared with the experimental value $\gamma_{qm} = 0.064$ cm⁻¹. The latter, leading to a scaled value $\gamma_{qma} = 0.32$, is in very good agreement with both semiclassical and Monte Carlo estimates as given by [30]. The quantitative agreement between the small- κ decay of correlations and the Lorentzian curve demonstrates explicitly that behavior in such a region is universal, with no dependence on the actual details of the geometry.

4-disk: For the four-disk scatterer, we use the results of Refs. [4,5] for comparison with the experimental data. Asymptotically, for large R ,

$$\gamma_{cl} \simeq \frac{1}{\sqrt{2}R} \ln(2\sqrt{2} \sigma). \quad (40)$$

The autocorrelation function for 4-disk data in the fundamental domain is displayed in Fig. 7, corresponding

to $a = 5$ cm and $R = 20\sqrt{2}$ cm. The value $\gamma_{qm} = 0.070$ cm⁻¹ compares pretty well with the estimate from Eq. (40), $\gamma_{cl} = 0.069$ cm⁻¹.

In Fig. 8, the experimental escape rates γ_{qm} of the 4-disk system are compared with the classical prediction γ_{cl} for several values of the ratio σ . Note that data are included for 17 configurations of the different reduced (1/8, 1/4, 1/2 and full space) representations of the 4-disk geometry shown in Fig. 4. The radius of the disks used was $a = 5$ cm for the 1/8th space, and $a = 2$ cm for the others. A relevant quantity is the abscissa of absolute convergence s_c for Eq. (17), which can also be estimated from the Ruelle ζ -function with the classical cycle weights t_p replaced by the corresponding semiclassical ones. s_c serves as a crude lower bound of the escape rate [30]. The latter is also shown in Fig. 8. s_c becomes negative for $R/a < 4.5$.

By comparing the results found for the escape rate while passing from 2- up to 4-disk scattering, progressively smaller values are obtained. In general, it is interesting to examine the variation of the escape parameter with increasing number n of scatterers. For $n \rightarrow \infty$, one obtains a so-called Lorentz scatterer [5]. We carried out experiments with $n = 20$, with corresponding (scaled) escape rate $\gamma_{qm} \simeq 0.05$, which is roughly an order of magnitude smaller than the three- or four-disk values. In agreement with physical intuition, this indicates that the system approaches a closed system when the number of disks becomes very large. Accordingly, the escape rate from the chaotic region is found to be quite small.

B. Non-universal features

For intermediate κ , the semiclassical prediction of Eq. (35) fails because of the presence of the periodic orbits, which leads to *non-universal* behavior. In the case of just one periodic orbit, one may express the full two-point correlation function as

$$C(\kappa) \propto \sum_{n=0}^{\infty} \frac{2\gamma}{(\kappa - n\Delta s)^2 + 4\gamma^2}, \quad (41)$$

where Δs denotes the spacing between resonances in the wave-vector domain. For example, for the two-disk problem discussed above (Sec. IVa), $\Delta s = 2\pi/(R - 2a)$, provided the space is probed through the antisymmetric A_2 -representation only [32]. Thus, the autocorrelation oscillates with period Δs . Very good agreement is found between experiment and theory for this integrable two-disk system (Fig. 5), where the expected value $\Delta s \simeq 0.21$ cm⁻¹ is identical with the observed oscillation period.

For the three-disk scatterer in the fundamental domain, the average length of the periodic orbit per period is roughly given by $(l_0 + l_1)/2$, the mean separation of the resonances being therefore

$$\overline{\Delta s_{FD}} = \frac{4\pi}{2R - (2 + \sqrt{3})a}. \quad (42)$$

The autocorrelation is expected to oscillate with a period roughly equal to $\overline{\Delta s_{FD}}$. The value $\overline{\Delta s_{FD}} = 0.25 \text{ cm}^{-1}$ predicted from Eq. (42) is in very good agreement with the scale of the oscillations in Fig. 6.

Let us finally discuss the four-disk scatterer. In the full space, the average length of the periodic orbits per period can be estimated as the average length of the eight periodic orbits, 12, 23, 34, 41, 1234, 1432, 13, 24, where 1, 2, 3, 4 are the labels of the four disks [26]. The mean separation between the resonances is then given approximately by

$$\overline{\Delta s_{full}} = \frac{2\pi}{(2 + 1/\sqrt{2})R - (3 + \sqrt{2})a}. \quad (43)$$

For the 4-disk system in the fundamental domain (one-eighth of the phase space), the average length of the periodic orbit per period is $(l_0 + l_1 + l_2)/3$, thus the mean separation is

$$\overline{\Delta s_{FD}} = \frac{6\pi}{(3 + \sqrt{2})R - 2(2 + \sqrt{2})a}. \quad (44)$$

The autocorrelation will oscillate with an approximate period equal to $\overline{\Delta s_{FD}}$, which indicates the deviation from the semiclassical theory due to the presence of the periodic orbits. Thus, the large wave-vector (or short time) behavior is system specific. The value of $\overline{\Delta s_{FD}} = 0.21 \text{ cm}^{-1}$ found from Eq. (44) is in good agreement with the scale of oscillations in Fig. 7.

Non-universal contributions can play in general a crucial role in determining the overall structure of the spectral autocorrelation, since they can be of the same order of the universal result of Random Matrix Theory. Semiclassical methods have recently provided an insightful tool in modeling non-universal properties in addition to universal ones [41]. Beside the general remarks mentioned above, the systematic identification of non-universal features, along with their interplay with the universal scattering properties, deserves a separate experimental investigation.

VII. DISCUSSION AND CONCLUSIONS

We presented an extensive experimental investigation of hard-disk chaotic scattering in microwave open cavities. The experiments provide a conceptually clean and direct realization of the n -disk open billiard problem. By exploiting our (in principle unlimited) capability to vary the geometry, chaotic scattering was studied in various configurations by both changing the number of disks and the symmetry properties of the underlying phase space.

Two main conclusions can be drawn from the experiments. First, the general validity and the predictive power of semiclassical methods have been tested directly by comparing the observed spectra with the corresponding semiclassical predictions. Qualitative agreement has been verified in all the situations investigated, and quantitative comparison found for a wide class of relatively sharp resonances. In addition, the experiments point out the validity of the wave-vector autocorrelation function as a probe for phase-space structure and quantum chaos. Values of wave-mechanical escape rates have been extracted from the observed autocorrelations, and compared to their classical counterparts. In general, the agreement observed between the measured escape parameters and the corresponding semiclassical predictions tends to be quantitatively superior than the one reachable in the detailed comparison of single resonance peaks. A similar conclusion has been reached for closed geometries where a much better agreement between experimental and numerical results has been obtained for the statistical properties rather than for the comparison of the individual resonances [42]. This feature reflects the nature of the escape rate as an average spectral property.

We remark that the present experiments, which probe wave-vector dependence, nicely complement measurements performed on semiconductor microstructures, where a similar role has been stressed for the magnetic field correlation of the two-point conductance. From the broader perspective of *quantum-classical correspondence*, the experiments shed light on the interplay between classical and quantum features of the scattering dynamics, by showing that measurable properties like quantum correlation lengths can be predicted from a knowledge of the classical chaotic scattering behavior.

Our investigation clearly points out, among other issues, the need for a deeper understanding of the non-universal properties of the spectral statistics and their interplay with universal ones. Such an investigation is likely to involve wave-vector autocorrelation functions as considered in the present analysis, as well as different quantities useful to characterize and probe the chaotic dynamics. In general, novel tools may be required in order to pull out the whole amount of information encapsulated in the observed spectra. Work is ongoing along these directions.

VIII. ACKNOWLEDGMENTS

This work was supported by NSF-PHY-9722681.

- [1] B. Eckhardt, J. Phys. A **20**, 5971(1987).
- [2] P. Cvitanović, Phys. Rev. Lett. **61**, 2729 (1988); P. Cvitanović and B. Eckhardt, *ibid.* **63**, 823 (1989).
- [3] P. Gaspard and S. A. Rice, J. Chem. Phys. **90**, 2225 (1989); **90**, 2242 (1989); **90**, 2255 (1989); **91**, E3279 (1989).
- [4] P. Gaspard and D. Alonso Ramirez, Phys. Rev. A **45**, 8383 (1992).
- [5] P. Gaspard, *Chaos, Scattering and Statistical Mechanics* (Cambridge University Press, Cambridge, 1998).
- [6] O. Bohigas, in: *Chaos and Quantum Physics*, edited by M.-J. Giannoni, A. Voros, and J. Zinn-Justin (Elsevier Science, New York, 1990), and references therein.
- [7] W. John, B. Milek, H. Schanz and P. Seba, Phys. Rev. Lett. **67**, 1949 (1991).
- [8] *Chaotic Scattering*, Special issue of CHAOS **3**, edited by T. Tél and E. Ott, pp. 417-706 (1993).
- [9] W. Lu, M. Rose, K. Pance, and S. Sridhar, Phys. Rev. Lett. **82**, 5233 (1999).
- [10] R. A. Jalabert, H. U. Baranger, and A. D. Stone, Phys. Rev. Lett. **65**, 2442 (1990).
- [11] B. Eckhardt, U. Dörr, U. Kuhl, and H.-J. Stöckmann, LANL e-print chao-dyn/9905005.
- [12] S. Sridhar, Phys. Rev. Lett. **67**, 785 (1991).
- [13] A. Kudrolli, S. Sridhar, A. Pandey, and R. Ramaswamy, Phys. Rev. E **49**, R11 (1994).
- [14] A. Kudrolli, V. Kidambi, and S. Sridhar, Phys. Rev. Lett. **75**, 822 (1995).
- [15] R. G. Newton, *Scattering Theory of Waves and Particles* (Springer, New York, 1982).
- [16] S. Sridhar, D. O. Hogenboom, and B. A. Willemsen, J. Stat. Phys. **68**, 239 (1992).
- [17] S. Datta, *Electronic Transport in Mesoscopic Systems* (Cambridge University Press, Cambridge, 1995).
- [18] Y. V. Fyodorov and B. A. Khoruzhenko, LANL e-print cond-mat/9903043.
- [19] J. Stein, H.-J. Stöckmann, and U. Stoffregen, Phys. Rev. Lett. **75**, 53 (1995).
- [20] C. M. Marcus, A. J. Rimberg, R. M. Westervelt, P. F. Hopkins, and A. C. Gossard, Phys. Rev. Lett. **69**, 506 (1992).
- [21] D. S. Fisher and P. A. Lee, Phys. Rev. B **23**, 6851 (1981).
- [22] W. A. Lin and R. V. Jensen, Phys. Rev. B **53**, 3638 (1996).
- [23] C. D. Schwieters, J. A. Alford, and J. B. Delos, Phys. Rev. B **54**, 10652 (1996), M. W. Beims, V. Kondratovich, and J. B. Delos, Phys. Rev. Lett. **81**, 4537 (1998).
- [24] R. Balian and C. Bloch, Ann. Phys. (N.Y.) **85**, 514 (1974).
- [25] M. C. Gutzwiller, *Chaos in Classical and Quantum Mechanics* (Springer, New York, 1990).
- [26] P. Cvitanović and B. Eckhardt, Nonlinearity **6**, 277 (1993); P. Cvitanović, R. Artuso, R. Mainieri, and G. Vattay, *Classical and Quantum Chaos: a Cyclist Treatise* (unpublished, 1998).
- [27] P. Gaspard and D. Alonso, T. Okuda, and K. Nakamura, Phys. Rev. E **50**, 2591 (1994).
- [28] J. V. José, C. Rojas, and E. J. Saletan, Am. J. Phys. **60**, 587 (1992).
- [29] A. Wirzba, CHAOS **2**, 77-83 (1992).
- [30] B. Eckhardt, G. Russberg, P. Cvitanović, P. E. Rosenqvist and P. Scherer, in: *Quantum chaos: between order and disorder*, edited by G. Casati and B. Chirikov (Cambridge University Press, 1995).
- [31] Y. Decanini, A. Folacci, E. Fournier and P. Gabrielli, J. Phys. A: **31**, 7865 (1998); **31**, 7891 (1998).
- [32] A. Kudrolli and S. Sridhar, in: *Proceedings of the 4th Drexel Symposium on Quantum Nonintegrability*, edited by D. H. Feng and B. L. Hu (International Press, Cambridge, MA, 1997).
- [33] C. Bercovich, U. Smilansky, and G. P. Farmelo, Eur. J. Phys. **12**, 122 (1991).
- [34] B. Eckhardt, CHAOS **3**(4), 616 (1993).
- [35] Y.-C. Lai, R. Blümel, E. Ott, and C. Grebogi, Phys. Rev. Lett. **68**, 3491 (1992).
- [36] Y. Alhassid and Y. Fyodorov, J. Phys. Chem. A **102**, 9577 (1998).
- [37] R. Blümel and U. Smilansky, Phys. Rev. Lett. **60**, 477 (1988); Physica (Amsterdam) **D 36**, 111 (1989); U. Smilansky, in: *Chaos and Quantum Physics*, edited by M.-J. Giannoni, A. Voros, and J. Zinn-Justin (Elsevier Science, New York, 1990), and references therein.
- [38] C. H. Lewenkopf and H. A. Weidenmüller, Ann. Phys. (N. Y.) **212**, 53 (1991).
- [39] T. Ericsson, Phys. Rev. Lett. **5**, 430 (1960).
- [40] D. M. Brink and R. O. Stephen, Phys. Lett. **5**, 77 (1963).
- [41] O. Agam, LANL e-print cond-mat/9812249.
- [42] H. Alt, C. Dembowski, H.-D. Gräf, R. Hofferbert, H. Rehfeld, A. Richter, and C. Schmit, Phys. Rev. E **60**, 2851 (1999).

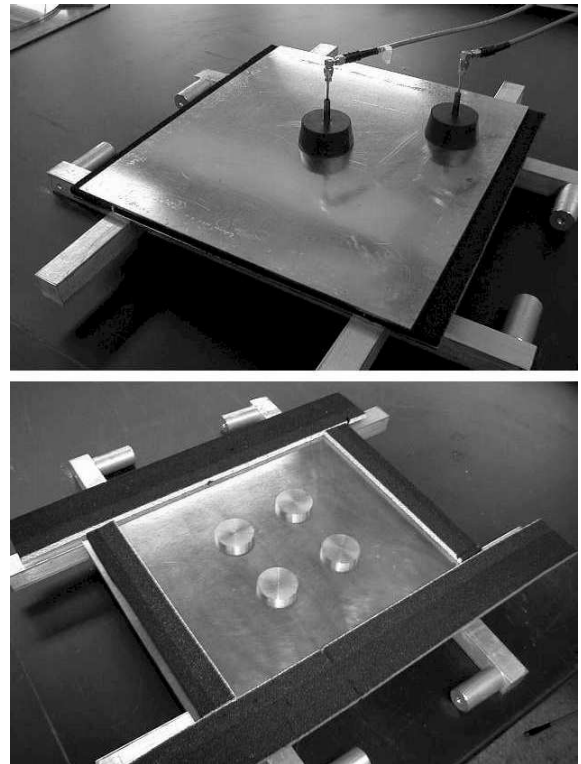


FIG. 1. Photo of the experimental apparatus. (Top) Closed cavity. (Bottom) Open cavity.

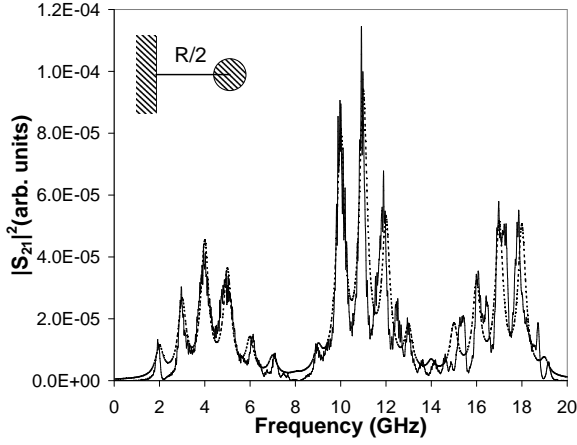


FIG. 2. Experimental (solid line) vs. semiclassical (dashed line) transmission function $|S_{21}|^2$ for a 2-disk system with $R = 40$ cm and $a = 5$ cm probed in the fundamental domain. (Inset) Sketch of the corresponding experimental configuration. The separation distance R is indicated.

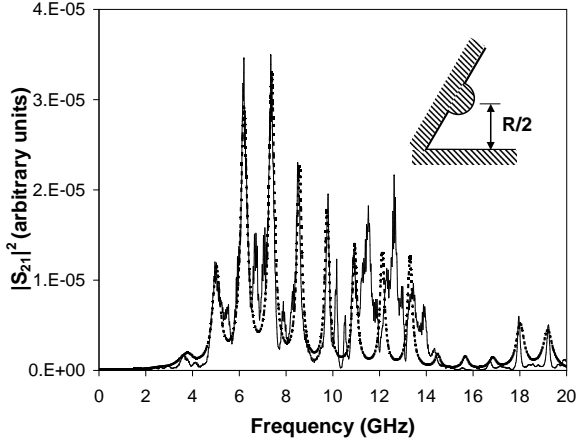


FIG. 3. Experimental (solid line) vs. semiclassical (dashed line) transmission function $|S_{21}|^2$ for a 3-disk system in the fundamental domain with $R = 20\sqrt{3}$ cm and $a = 5$ cm. The corresponding experimental configuration is sketched in the inset. The separation distance R is indicated.

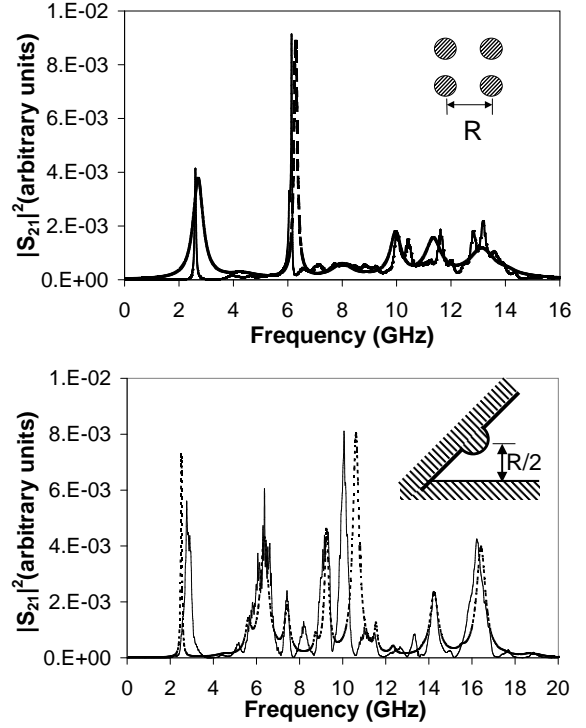


FIG. 4. Experimental (solid line) vs. semiclassical (dashed line) transmission function $|S_{21}|^2$ for a 4-disk system. (Top) Full space geometry with $R = 8$ cm and $a = 2$ cm. (Bottom) $1/8$ th space (fundamental domain) with $R = 20$ cm and $a = 5$ cm. The corresponding experimental configurations are sketched in the insets. The separation distance R is indicated.

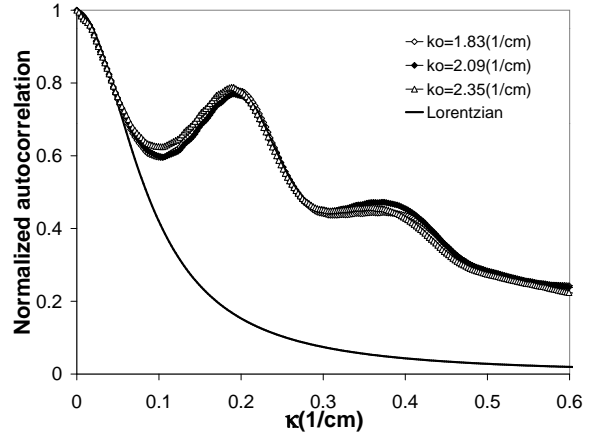


FIG. 5. Wave-vector autocorrelation $C(\kappa)$ of the 2-disk system with $R=40$ cm and $a=5$ cm. Data are shown for the half-space configuration of the 2-disk geometry, corresponding to the A_2 representation. The correlation is calculated with interval $\Delta k = 3$ cm^{-1} . The different sets represent different values of the central wave-vector k_0 . The bold line is a Lorentzian with $\gamma_{qm}=0.083$ cm^{-1} .

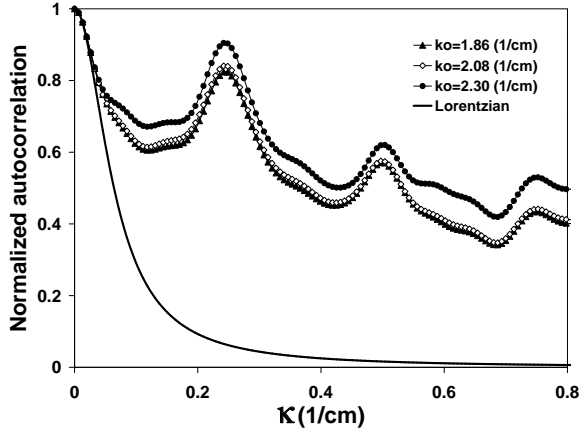


FIG. 6. Wave-vector autocorrelation $C(\kappa)$ of the 3-disk system with $R = 20\sqrt{3}$ cm and $a = 5$ cm. Data are taken in the fundamental domain, corresponding to the A_2 representation. The correlation is calculated with interval $\Delta k = 2$ cm^{-1} . The different sets represent different values of the central wave-vector k_0 . The bold line is a Lorentzian with $\gamma_{qm} = 0.064$ cm^{-1} .

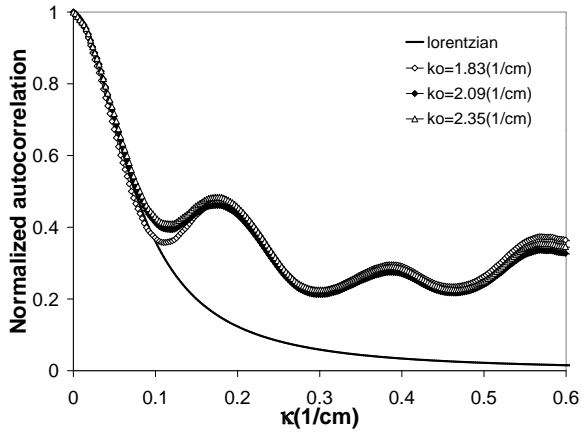


FIG. 7. Wave-vector autocorrelation $C(\kappa)$ of the 4-disk system with $R = 20\sqrt{2}$ cm and $a = 5$ cm. Data are taken in the fundamental domain, corresponding to the B_2 representation. The correlation is calculated with interval $\Delta k = 3$ cm^{-1} . The different sets represent different values of the central wave-vector k_0 . The bold line is a Lorentzian with $\gamma_{qm} = 0.070$ cm^{-1} .

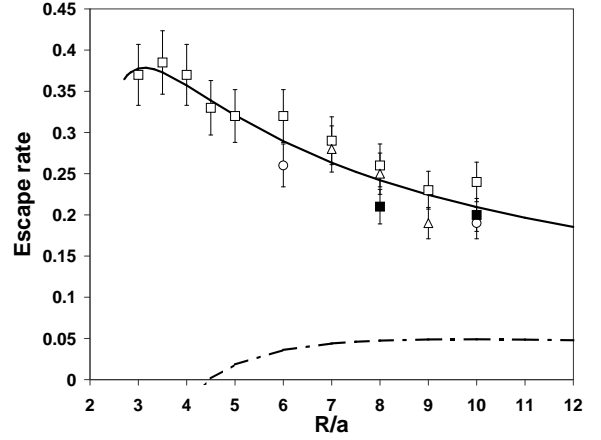


FIG. 8. Experimental escape rate γ_{qm} scaled to radius $a = 1$ vs. ratio $\sigma = R/a$. Data are shown for different reduced configurations of the 4-disk geometry: 1/8th space (open squares), 1/2 space (open circles), 1/4th space (filled squares), full space (triangles). The classical escape rate (solid line) is calculated from the first 3 periodic orbits in the fundamental domain. The abscissa of convergence s_c of Eq. (17), which is shown as a dot-dashed line, represents a lower bound on the quantum escape rate.